Catalysis Communications 73 (2016) 123–127

Contents lists available at ScienceDirect

Catalysis Communications

journal homepage: www.elsevier.com/locate/catcom

Short communication

Low-temperature efficient degradation of ethyl acetate catalyzed by lattice-doped CeO_2–CoO_x nanocomposites

Sadia Akram [a,b,1], Zhen Wang [a,1], Lan Chen [a], Qi Wang [a,*], Genli Shen [a], Ning Han [c], Yunfa Chen [c], Guanglu Ge [a,*]

[a] CAS Key Laboratory of Standardization and Measurement for Nanotechnology, National Centre for Nanoscience and Technology, No. 11 Zhongguancun Beiyitiao, Beijing 100190, China
[b] University of Chinese Academy of Science, No. 19A Yuquan Road, Beijing 100049, China
[c] State Key Laboratory of Multiphase Complex Systems, Institute of Process Engineering, Chinese Academy of Sciences, Beijing 100190, China

ARTICLE INFO

Article history:
Received 8 July 2015
Received in revised form 14 October 2015
Accepted 19 October 2015
Available online 20 October 2015

Keywords:
Ethyl acetate oxidation
Ce–Co composite oxides
Hydrothermal method
Redox properties
Lattice oxygen

ABSTRACT

A series of CeO_2–CoO_x nanocatalysts have been synthesized by a facile surfactant-free hydrothermal method and investigated for the oxidative degradation of ethyl acetate (EA) at exceptionally low temperature. The combination of various techniques, such as H_2-TPR, XRD, XPS and HRTEM provides insights to the effect of various factors including redox properties, enhanced lattice oxygen and its mobility *etc.* on catalysis performance. The results demonstrate that the enriched lattice oxygen is the dominant factor for the low-temperature degradation of EA due to the interaction between lattice-mixed Ce and Co ions, which can be used to design the catalysts for removing VOCs with improved performance.

© 2015 Elsevier B.V. All rights reserved.

1. Introduction

Volatile organic compounds (VOCs) are one of the most hazardous classes of organic pollutants. They are emitted from various anthropogenic activities and cause many environmental problems such as the formation of photochemical smog and the depletion of stratospheric ozone [1–4]. Ethyl acetate (EA) is one of the most common, ascendant and stable volatile organic solvents. Its long term exposure can cause severe health problem to human beings. This hazardous nature of EA urges the researchers to fabricate new materials and seek better approaches to its complete removal [5,6].

Catalytic combustion has been recognized as an efficient technology for EA degradation, where both noble and transition metals have been used as catalysts. However, transition metal oxides are more active for the oxidation of oxygenated VOCs besides their thermal stability and low cost, and are not prone to sintering and poisoning. Recently, CeO_2–CoO_x composites have attracted special attention in catalytic removal of numerous VOCs, which demonstrate higher catalytic activity than their individual components [7–12].

Although many works have been done previously, to develop a system to degrade EA at reduced temperature is still needed. Therefore, to elucidate the low-temperature catalytic activity of the CeO_2–Co_3O_4 composites towards the oxidative degradation of EA is the main aim of this work. Herein, the difference in catalytic activities by varying molar ratios of Ce–Co is compared and evaluated, and the attention is also paid to analyze the interaction between CeO_2 and Co_3O_4 and the effect on its redox property, lattice oxygen storage and mobility.

2. Experimental

A facile surfactant-free hydrothermal method is used to prepare the catalysts and the detailed procedure is provided in Supporting Information (SI).

3. Results and discussion

3.1. Catalytic performance

Fig. 1a shows the degradation of EA over pure and composite oxides. The catalytic activity decreases in the order $Ce_{0.5}Co_{0.5}$ > $Ce_{0.7}Co_{0.3}$ > $Ce_{0.3}Co_{0.7}$ > CeO_2 > Co_3O_4. The temperature of 50 and 90% of EA conversion, T_{50} is 178, 184, 186, 189, and 218 °C while T_{90} is 195, 208, 211, 215 and 244 °C respectively. All other catalysts display higher T_{100} (total conversion) for EA oxidation than $Ce_{0.5}Co_{0.5}$ (T_{100} = 200 °C). The activity follows the same trend for these catalysts even at lower temperature. In addition, the superiority of $Ce_{0.5}Co_{0.5}$ among all the catalysts is confirmed by calculating the reaction rate of the samples at 156 °C (EA conversion <20%) as shown in Table S1, where $Ce_{0.5}Co_{0.5}$ shows the best catalytic performance that may be attributed to the stronger interaction between CeO_2 and Co_3O_4 due to the doping of Co_3O_4 in an appropriate ratio into

* Corresponding authors.
E-mail addresses: wangq@nanoctr.cn (Q. Wang), gegl@nanoctr.cn (G. Ge).
[1] These authors contributed equally.

http://dx.doi.org/10.1016/j.catcom.2015.10.024
1566-7367/© 2015 Elsevier B.V. All rights reserved.

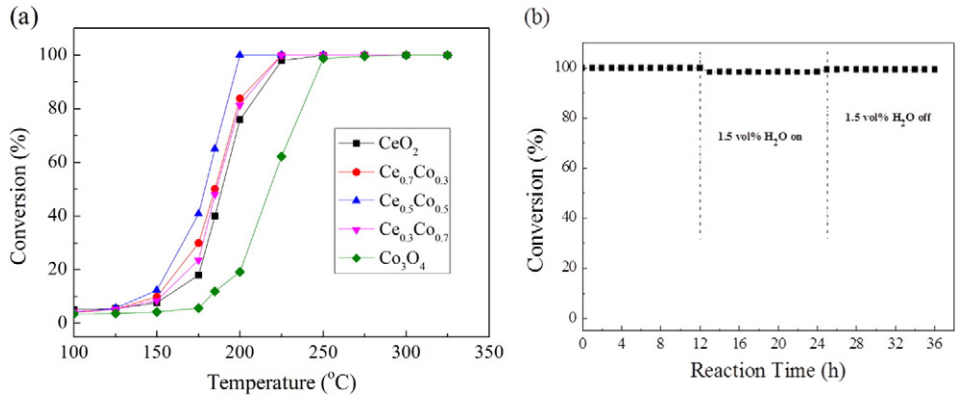

Fig. 1. Ethyl acetate conversion as a function of temperature over CeO_2, Co_3O_4 and $Ce_x Co_{1-x}$ catalyst (a) and effect of moisture on catalytic performance of $Ce_{0.5}Co_{0.5}$ catalyst at 200 °C (b).

CeO_2 lattice. This assumption will be further discussed in the following sections. In addition, the catalytic efficiency of the composite oxide is compared with other groups' works for the combustion of EA under similar conditions as shown in SI (Table S2).

$Ce_{0.5}Co_{0.5}$ is used to investigate the effect of the moisture and space velocity on the oxidative degradation of EA due to its best performance among all catalysts. Fig. 1b demonstrates that the moisture has a negative effect on the catalysis. However, in the absence of moisture the catalytic performance recovers and remains constant for further 12 h. This inhibitory effect of the moisture indicates that the water molecules may compete with EA to adsorb on the surface of the catalyst during catalysis. In addition, the increase of the gas flow rate (Fig. S1) appears to be another negative effect on the catalytic performance which can be attributed to the shortened time of interaction between the catalyst and the VOC.

3.2. Catalyst characterization

The crystal phases are determined by XRD. Fig. 2a confirms that the catalysts possess fluorite phase of CeO_2 (JCPDS # 81–0792) and spinal structure of Co_3O_4 (JCPDS # 74–2120) respectively. The addition of Co to CeO_2 causes the change in the structural (Table S3) and textural properties of the final products (Table S4). The decreased lattice parameter suggests that Co^{3+} or Co^{2+} ions are incorporated into CeO_2 lattice to form a solid solution, since the effective ionic radius of Co^{3+} (0.065 nm) or Co^{2+} (0.082 nm) is smaller than that of Ce^{4+} (0.111 nm), these findings are in a good agreement with the Raman analysis (Fig. S2 and S3). In addition, the characteristic peak of CeO_2 (111) at 28.6° gradually shifts towards the higher value as the cobalt content increases (Fig. 2b). The decreased lattice parameters of ceria are the evidence of solid solution formation [13]. However, the incorporation of cobalt ions in ceria framework leads to the formation of CeO_2–Co_3O_4 solid solution and the enhanced oxygen mobility due to increased oxygen vacancies [14] and will be discussed in the following paragraphs.

Fig. 3a shows that pure CeO_2 exhibits nanorod-like morphology while $Ce_{0.5}Co_{0.5}$ composite oxide shows a mixture of nanorods and particles (Fig. 3b), where the nanoparticles are confirmed as Co_3O_4- and the nanorods are CeO_2-enriched phases as determined by HRTEM (Fig. 3e). Pure Co_3O_4 has hollow donut-like morphology (Fig. 3c). Lattice fringes (Fig. 3d) in HRTEM are 0.31 nm corresponding to the $d(111)$ of CeO_2 and 0.46 nm assigned to (111) of Co_3O_4 (Fig. 3f). The EDS spectra of $Ce_{0.5}Co_{0.5}$ composite oxide are provided in SI (Fig. S4). Typical HAADF images are displayed in Fig. 3g. Taking all these HAADF information into account, it can observe that both Ce and Co are homogeneously dispersed across the whole $Ce_{0.5}Co_{0.5}$ catalyst, which is crucial for the enhanced oxygen storage and mobility, that in turn, affects the catalytic activity.

The oxidation state of catalyst surface species is examined by XPS analysis. Owing to the similarities in XPS patterns of all the samples, (Fig. S5) the pattern of $Ce_{0.5}Co_{0.5}$ is chosen as the representative for

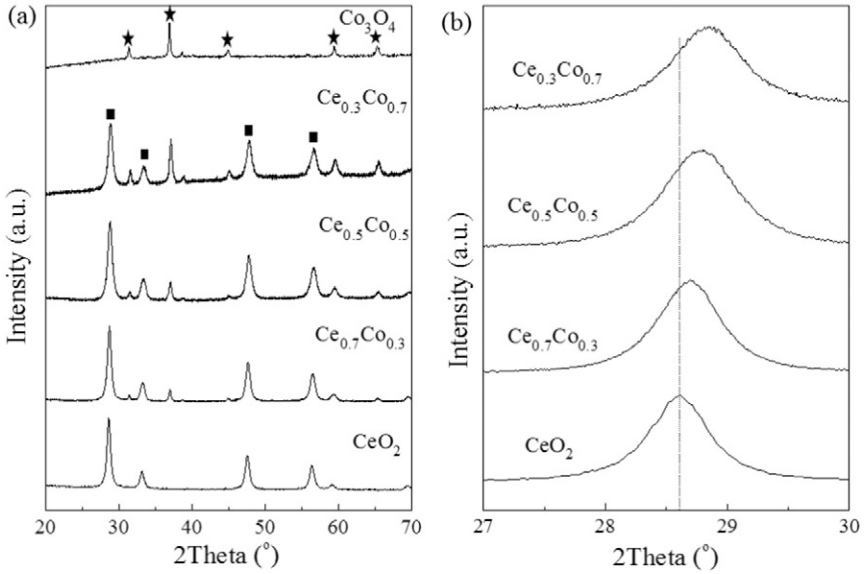

Fig. 2. XRD patterns of CeO_2, Co_3O_4 and Ce_xCo_{1-x} composite oxides: (a) wide angle patterns, and (b) enlarged zone patterns. Crystalline phases detected: Co_3O_4 (*) and CeO_2 (■).

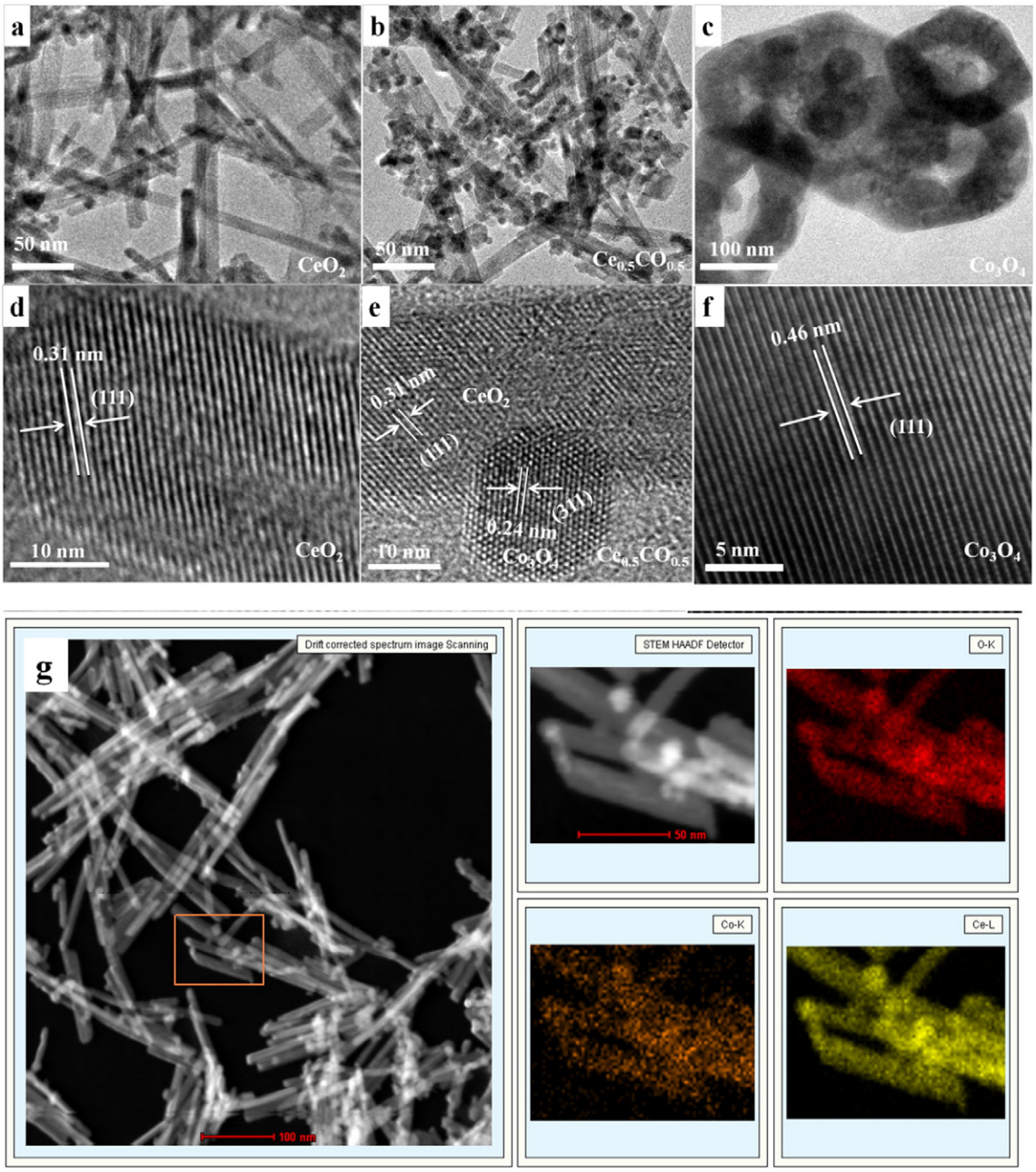

Fig. 3. TEM, HRTEM images of CeO_2 (a, d), $Ce_{0.5}Co_{0.5}$ (b, e), Co_3O_4 (c, f) and High Angle Annular Dark Field mapping (HAADF) micrographs of $Ce_{0.5}Co_{0.5}$ (g).

the following discussion. Fig. 4a represents the XPS patterns for Ce 3d core level of $Ce_{0.5}Co_{0.5}$. In these patterns, six peaks labeled as V_0 (881.9 eV), V_1 (888.5 eV), V_2 (897.8 eV), V_0' (900.8 eV), V_1' (907.3 eV) and V_2' (916.2 eV) can be assigned to the characteristic profile of Ce^{4+} 3d final states [15,16]. The high binding energy (BE) doublet (V_2/V_2') is attributed to the final state of Ce (IV) $3d^94f^0O2p^6$, doublet V_1/V_1' is originated from the state of Ce (IV) $3d^94f^1O2p^5$, and doublet V_0/V_0' corresponds to the state of Ce (IV) $3d^94f^2O2p^4$. The characteristic peaks of Ce^{3+} are also observed at 903.3/884.6 eV and 897.9/879.2 eV labeled as U_1/U_1' and U_0/U_0', respectively. The content of Ce^{4+} is estimated to be 0.806 based on integrated peak area. Therefore, Ce species exist mainly in tetravalent oxidation state [17].

Fig. 4b exhibits the Co 2p XPS pattern of $Ce_{0.5}Co_{0.5}$. It is quite difficult to distinguish Co^{2+} and Co^{3+} due to the small difference in their BEs. The spin–orbit splitting of the Co 2p peaks (ΔE) is found to be well correlated with the cobalt oxidation state [18] calculated by Formula (1). The ΔE value is 16.0 eV for CoO [19], 15.0 eV for the cobaltic compounds (Co_2O_3), and 15.2 eV for the mixed-valence Co_3O_4 [18]. All the catalysts have ΔE = 15.2 eV, so Co_3O_4 is considered as the main phase in pure cobalt oxide which conforms XRD and HRTEM analysis.

$$\Delta E = E\left(Co\ 2p_{1/2}\right) - E\left(Co\ 2p_{3/2}\right) \quad (1)$$

The O 1s spectra of $Ce_{0.5}Co_{0.5}$ (Fig. 4c) show the peaks at low (529.0 eV) and medium (531.0 eV) BEs indicating lattice (O^{2-}) and surface adsorbed oxygen species (O^{2-}, O^-, O_2^{2-}) respectively. Besides this, a broad shoulder at high BE (533.5 eV) refers to the contribution of the defective oxides or the presence of hydroxylated or carbonated oxygen on the surface of the catalysts [20]. The relative ratio of O_α/O_β for all catalysts in terms of the lattice oxygen to surface species is summarized in Table 1 and Fig. 4d, which shows that $Ce_{0.5}Co_{0.5}$ possesses the highest ratio of O_α/O_β. This property confirms the evidence of the enhanced lattice oxygen storage and mobility incurred by the strong CeO_2–Co_3O_4

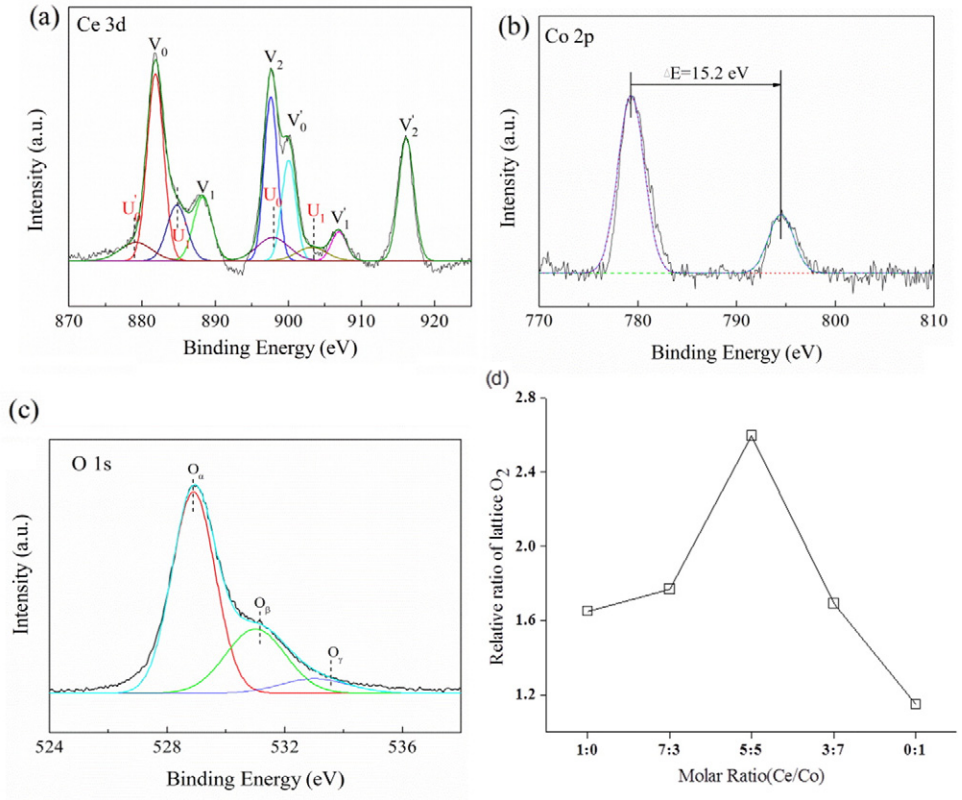

Fig. 4. XPS in the Ce 3d (a), Co 2p (b), O 1s (c) regions in $Ce_{0.5}Co_{0.5}$ composite oxide and the relative ratio of lattice O_2 (d) in pure and Ce_xCo_{1-x} composite oxides respectively.

interaction which facilitates the oxidation of EA [11]. Moreover, lifetime Positron annihilation study (Table S5) indicates that the oxygen vacancies increase in $Ce_{0.5}Co_{0.5}$ compared with pure ceria due to Co ions doping into the crystal lattice of CeO_2, which is consistent with the XRD and Raman analysis. Taking all the cases into account, it can be concluded that the increased lattice oxygen and oxygen vacancies are the determinant factor responsible for the enhanced oxidative degradation of EA over $Ce_{0.5}Co_{0.5}$. The synergistic effect of the transition metal doped CeO_2 catalysts on their catalytic activity has been evaluated [13,21], where the replacement of Ce^{4+} by the secondary metal cations in ceria lattice results in the change of the lattice oxygen defect and vacancy concentration, and the improved catalytic performance.

Table 1 demonstrates the comparison between XPS and ICP-MS for the elemental composition along with the dispersion of Ce ions on the surface and in the bulk of the catalysts. In case of the composite oxides, the atomic ratio of Ce/Co is lower in the bulk than that on the surface. For $Ce_{0.5}Co_{0.5}$ catalyst, the value of the bulk Ce/Co atomic composition is closest to that of the surface molar ratio of Ce/Co indicating that CeO_2 and Co_3O_4 are homogeneously distributed in either bulk or surface. This implies the interaction between CeO_2 and Co_3O_4 species reaches to the maximum at this ratio and leads to the increased oxygen storage and mobility. The result is in a good agreement with lattice oxygen contents (O_α) calculated by XPS.

To determine the effect of cobalt doping on the redox nature of CeO_2–CoO_x nanocomposites, H_2-TPR analysis is carried out as shown in Fig. 5. Pure CeO_2 shows two reduction peaks at 477 and 725 °C. The lower and higher temperature peaks are attributed to the reduction of surface oxygen species and bulk reduction of CeO_2 by the removal of anionic oxygen from the lattice and formation of Ce_2O_3, respectively [23,24]. Pure Co_3O_4 has an intense peak centered at 308 °C with a shoulder around 270 °C [25]. This feature corresponds to the two step reduction of Co_3O_4. Low-temperature peak refers to the reduction of Co^{3+} ions to Co^{2+} accompanying the structural change from Co_3O_4 to CoO (Eq. (2)), while high temperature peak indicates the CoO reduction to metallic cobalt (Eq. (3)) [11].

$$Co_3O_4 + H_2 \rightarrow 3CoO + H_2O \quad (2)$$

$$CoO + H_2 \rightarrow Co + H_2O \quad (3)$$

For the composite oxides, TPR profile is more complex than the pristine. The reduction start from 200 °C and is completed up to 500 °C. Two overlapping peaks from 200 to 400 °C are ascribed to the step-wise reduction of Co^{3+} to Co^{2+} and then to Co^0. Besides the reduction of cobalt ions, reduction of surface Ce^{4+} to Ce^{3+} also occurs at the same time. As a result, two important observations can be drawn: (1) all the composite oxides exhibit increased reducibility at lower temperature than pure CeO_2 as the TPR-H_2 reduction peaks at higher temperature dramatically shift towards the lower temperature with the addition of Co_3O_4, (2) the composite oxides show higher oxygen mobility both on the surface and within the bulk due to the addition of Co content. These observations suggest that Co_3O_4 is able to enhance the reducibility of CeO_2 owing to

Table 1
XPS results and Co/Ce atomic ratio of Ce_xCo_{1-x} samples.

Sample	BE (eV)		Ratio of O_α/O_β	Atomic ratio of Ce/Co	
	O_α	O_β		ICP	XPS[a]
CeO_2	529.0	531.5	1.64957		
$Ce_{0.7}Co_{0.3}$	529.1	531.3	1.76923	1.6	2.54
$Ce_{0.5}Co_{0.5}$	529.0	531.2	2.59688	1.08	1.26
$Ce_{0.3}Co_{0.7}$	529.2	531.3	1.69129	0.37	0.70
Co_3O_4	529.6	531.6	1.14834		

[a] Refined by their Atomic Sensitivity Factors (ASF), 3.59 for Co 2p and 8.81 for Ce 3d [22].

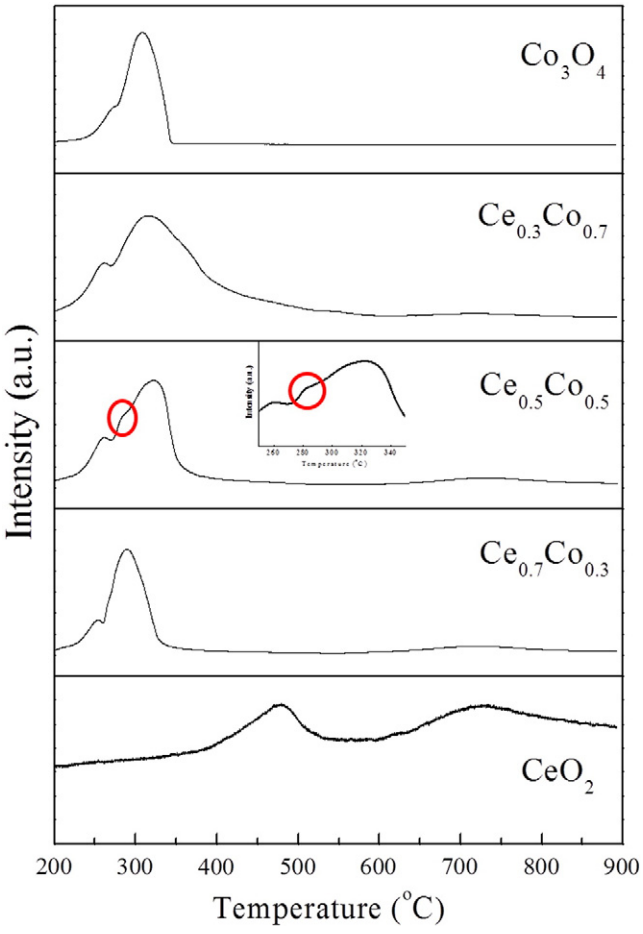

Fig. 5. H_2-TPR profiles of CeO_2, Co_3O_4 and $Ce_x\,Co_{1-x}$ composite oxides.

strong interaction between Co_3O_4 and CeO_2. Numerous studies have also been conducted to examine the similar effect indicating that the decrease in reduction temperature of metal oxide can be achieved by the addition of another metal [10,11,26].

From the TPR profile, it shows that $Ce_{0.5}Co_{0.5}$ exhibits different reduction behavior from others. A small shoulder between the two peaks at lower temperature (Fig. 5) can be assigned to the strong interaction between CeO_2 and Co_3O_4 resulting in the unique redox properties, which is a key factor responsible for the enhanced catalytic activity. Another possible reason for the unique redox properties of this candidate is the atomic ratio of Ce/Co close to 1 (Table 1), which results in the well-dispersion of Co species surrounding Ce atom. The findings are consistent with the HADAF mapping analysis. Furthermore, a comparison between theoretical and actual hydrogen consumption of pure Co_3O_4 and composite oxides is made in Table S6. Actual consumption of hydrogen is slightly higher than the theoretically calculated value for the pure and the composite oxides. In case of composite oxides, the excess hydrogen is thought to be consumed for the partial CeO_2 reduction and the H_2 spillage over CeO_2 support [26], while for the pure Co_3O_4 it represents the complete reduction of Co_3O_4 to metallic cobalt.

4. Conclusion

Catalytic oxidation of EA has been conducted over pure and composite Ce/Co oxides. The insertion of cobalt ions in CeO_2 lattice results in the loss of the charge equilibrium and increases the available lattice oxygen in bulk. These properties play a vital role in the superior catalytic activity of Ce–Co composite oxides, particularly $Ce_{0.5}Co_{0.5}$ towards catalytic oxidation. The oxidative degradation leads to a complete conversion of EA to CO_2 and H_2O with higher efficiency at reduced temperature. Our research opens an alternative way for the further application of Ce–Co nanocomposites in the degradation of other VOCs.

Acknowledgments

The authors thank National Natural Science Foundation of China (No. 51402061), Strategic pilot projects for science and technology of CAS (No. XDB05050000), National Science & Technology Pillar Program (No. 20114BAC021B00) for financial support. We also acknowledge Open Research Fund of State Key Laboratory of Multiphase Complex Systems (No. Y52501A12D).

Appendix A. Supplementary data

Supplementary data to this article can be found online at http://dx.doi.org/10.1016/j.catcom.2015.10.024.

References

[1] K. Unger, Science 312 (2006) 823.
[2] R.R. Matheson, Science 297 (2002) 976.
[3] G.H. Hutch, C.S. Heneghan, L.D. Hudson, S.H. Taylor, Nature 384 (1996) 341.
[4] S.K. Ihm, Environ. Eng. Res. 4 (2000) 213.
[5] Occupational health Guideline for Ethyl Acetate (1978) U.S. Department of Labor, Occupational Safety and Health Administration.
[6] T. Tsoncheva, M. Linden, S. Areva, C. Minchev, Catal. Commun. 7 (2006) 357.
[7] N. Kamiuchi, T. Mitsui, H. Muroyama, T. Matsui, R.K. Eguchi, Appl. Catal. B Environ. 97 (2010) 120.
[8] X.W. Su, L.Y. Jin, J.Q. Lu, M.F. Luo, J. Ind. Eng. Chem. 15 (2009) 683.
[9] S.S.T. Bastos, S.A.C. Carabineiro, J.J.M. Orfao, M.F.R. Pereira, J.J. Delgado, J.L. Figueiredo, Catal. Today 180 (2012) 148.
[10] X. Chen, S.A.C. Carabineiro, S.S.T. Bastos, P.B. Tavares, J.J.M. Orfao, M.F.R. Pereira, J.L. Figueiredo, J. Environ. Chem. Eng. 2 (2014) 344.
[11] L.F. Liotta, M. Ousmane, G.D. Carlo, G. Pantaleo, G. Deganello, G. Marci, L. Retailleau, A.G. Fendler, Appl. Catal. A Gen. 347 (2008) 81.
[12] X. Chen, S.A.C. Carabineiro, S.S.T. Bastos, P.B. Tavares, J.J.M. Orfao, M.F.R. Pereira, J.L. Figueiredo, Appl. Catal. A Gen. 472 (2014) 101.
[13] Z. Wang, G. Shen, J. Li, H. Liu, Q. Wang, Y. Chen, Appl. Catal. B Environ. 138 (2013) 253.
[14] L.F. Liotta, G.D. Carlo, G. Pantaleo, G. Deganello, Appl. Catal. B Environ. 70 (2007) 314.
[15] A. Pfau, K.D. Schierbaum, Surf. Sci. 321 (1994) 71.
[16] W.D. Xiao, Q.L. Guo, E.G. Wang, Chem. Phys. Lett. 368 (2003) 527.
[17] F. Lenormand, L. Hilaire, K. Kili, G. Krill, G. Maire, J. Phys. Chem. 92 (1988) 2561.
[18] K. Ichimura, Y. Inoue, I. Yasumori, Bull. Chem. Soc. Jpn. 53 (1980) 3044.
[19] J.Y. Luo, M. Meng, X. Li, X.G. Li, Y.Q. Zha, T.D. Hu, Y.N. Xie, J. Zhang, J. Catal. 254 (2008) 310.
[20] W. Tang, X. Wu, D. Li, Z. Wang, H. Liu, Y. Chen, J. Mater. Chem. A 2 (2014) 2544.
[21] L.F. Liotta, G.D. Carlo, G. Pantaleo, A.M. Venezia, G. Deganello, Appl. Catal. B Environ. 66 (2006) 217.
[22] C.D. Wagner, W.M. Riggs, L.E. Davis, J.F. Moulder, G.E. Muilenberg, Handbook of X-ray Photoelectron Spectroscopy, Perkin-Elmer, Eden Praine, MN, 1979 253.
[23] K. Zhou, X. Wang, X. Sun, Q. Peng, Y. Li, J. Catal. 229 (2005) 206.
[24] S.A.C. Carabineiro, X. Chen, M. Konsolkis, A.C. Psarras, P. Tavares, J.J.M. Orfao, M.F.R. Pereira, J.L. Figueiredo, Catal. Today 244 (2015) 161.
[25] C.F. Yan, H. Chen, R.R. Hu, S. Huang, W. Luo, C. Guo, M. Li, W. Li, Int. J. Hydrog. Energy 39 (2014) 18695.
[26] M. Konsolkis, M. Sgourakis, S.A.C. Carabineiro, Appl. Surf. Sci. 341 (2015) 48.